Invariance property of the Fisher information in scattering media: supplementary material

Michael Horodynski,[1] Dorian Bouchet,[2] Matthias Kühmayer,[1] and Stefan Rotter[1]

[1] *Institute for Theoretical Physics, Vienna University of Technology (TU Wien), 1040 Vienna, Austria*
[2] *Université Grenoble Alpes, CNRS, LIPhy, 38000 Grenoble, France*

I. DERIVATION OF EQ. (3)

Here we provide the detailed derivation of the main result presented in Eq. (3) of the main text. Our starting point is the decomposition of the generalized Wigner-Smith (GWS) operator into the Green's function G, the coupling matrix to the leads V and the perturbation of the potential function describing the scattering landscape ΔH [1],

$$Q_\theta = \frac{2}{\Delta\theta} V^\dagger G^\dagger \Delta H G V \,, \tag{S1}$$

where $\Delta\theta$ quantifies the (infinitesimal) change in the parameter of interest. In order to find the average Fisher information we need an expression for the trace of the Fisher information operator, which, in turn, is proportional to the trace of the squared GWS operator, i.e.,

$$\begin{aligned} \operatorname{Tr} F_\theta &= \frac{4}{\Delta\theta^2} \operatorname{Tr}\left[V^\dagger G^\dagger \Delta H G V V^\dagger G^\dagger \Delta H G V\right], \\ &= \frac{4}{\Delta\theta^2} \operatorname{Tr}\left\{\left[\operatorname{Im}(G)\,\Delta H\right]^2\right\}, \end{aligned} \tag{S2}$$

where we have used the identity $GVV^\dagger G^\dagger = -\operatorname{Im} G$ which is derived from $SS^\dagger = \mathbb{1}$ to arrive at the second line of Eq. (S2).

We now turn our attention to a specific perturbation, namely the shift of a sub-wavelength particle which we characterize by $\Delta H = k^2(\varepsilon_T - 1)[\delta(\mathbf{r} - \mathbf{r}_T - \Delta\mathbf{r}) - \delta(\mathbf{r} - \mathbf{r}_T)]$, where $\mathbf{r}_T$ is the position of the target and $\Delta\mathbf{r}$ is an infinitesimal displacement. Putting this ΔH into Eq. (S2) we get:

$$\begin{aligned} \operatorname{Tr} F_x =& \frac{4k^4(\varepsilon_T - 1)^2}{\Delta x_T^2} \Big[\operatorname{Im} G\left(\mathbf{r}_T, \mathbf{r}_T; k^2\right)^2 \\ &- 2\operatorname{Im} G\left(\mathbf{r}_T, \mathbf{r}_T + \Delta\mathbf{r}; k^2\right)^2 \\ &+ \operatorname{Im} G\left(\mathbf{r}_T + \Delta\mathbf{r}, \mathbf{r}_T + \Delta\mathbf{r}; k^2\right)^2\Big]. \end{aligned} \tag{S3}$$

In this equation we now identify the Green's function G with the so-called cross density of states (CDOS) [2, 3] defined as

$$\rho_{12}(k) = -\frac{2k}{\pi} \operatorname{Im} \widetilde{G}\left(\mathbf{r}_1, \mathbf{r}_2; k^2\right), \tag{S4}$$

where $\widetilde{G}(\mathbf{r}_1, \mathbf{r}_2) = \varepsilon(\mathbf{r}_1)^{1/2} G(\mathbf{r}_1, \mathbf{r}_2) \varepsilon(\mathbf{r}_2)^{1/2}$ denotes the Green's function suitably defined to calculate the LDOS [4]. Plugging the CDOS into Eq. (S3) we then get

$$\operatorname{Tr} F_x = \frac{2k^2(\varepsilon_T - 1)^2 \pi^2}{\varepsilon_T^2 \Delta x_T^2} \left(\rho_{11}^2 - \rho_{12}^2\right), \tag{S5}$$

$$\langle \operatorname{Tr} F_x \rangle = \frac{k^4(\varepsilon_T - 1)^2 \pi^2}{\varepsilon_T^2} \langle \rho_{11}^2 \rangle, \tag{S6}$$

where we used the observation that for short distances the CDOS follows on average a simple law, irrespective of the surrounding scattering environment [3] to arrive at Eq. (S6),

$$\begin{aligned} \langle \rho_{12}^2 \rangle =& J_0(k\Delta x_T)^2 \langle \rho_{11}\rho_{22} \rangle & \text{(S7)} \\ \approx& \left(1 - k^2 \Delta x_T^2/2\right) \langle \rho_{11}\rho_{22} \rangle, & \text{(S8)} \end{aligned}$$

where J_0 is the zeroth-order Bessel function of the first kind and we identify $\rho_{11} \equiv \rho(\mathbf{r}_T, k)$.

In the case of measuring the dielectric constant, the perturbation is given by $\Delta H = k^2 \Delta\varepsilon_T \delta(\mathbf{r} - \mathbf{r}_T)$. Employing the same reasoning as the one presented above in the case of position estimations, we obtain

$$\langle \operatorname{Tr} F_\varepsilon \rangle = \frac{k^2 \pi^2}{\varepsilon_T^2} \langle \rho_{11}^2 \rangle. \tag{S9}$$

This implies that the same invariance property as for F_x also exists for measurements on the dielectric constant (apart from a different prefactor).

II. DETAILED ANALYSIS OF LDOS SCALING

Here we provide the detailed argument, why the Fisher information scales quadratically with the LDOS in the unitary case, while it scales linearly for non-unitary scattering matrices. We start by considering the derivative of the scattering matrix with respect to some arbitrary parameter:

$$\partial_\theta S = -2iV^\dagger G \Delta H G V / \Delta\theta, \tag{S10}$$

This gives us the following expression for the Fisher information operator:

$$\begin{aligned} F_\theta =& \frac{4}{\Delta\theta^2} V^\dagger G^\dagger \Delta H G^\dagger V V^\dagger G \Delta H G V & \text{(S11)} \\ =& -\frac{4}{\Delta\theta^2} V^\dagger G^\dagger \Delta H \operatorname{Im}(G) \Delta H G V & \text{(S12)} \\ =& \frac{2\pi}{k\Delta\theta^2} V^\dagger G^\dagger \Delta H \varepsilon^{-1/2} \rho \varepsilon^{-1/2} \Delta H G V, & \text{(S13)} \end{aligned}$$

where we use $G^\dagger V V^\dagger G = -\,\mathrm{Im}(G)$, which follows from $S^\dagger S = \mathbb{1}$ to arrive at Eq. (S12). We reach Eq. (S13) by first transforming G to $\widetilde{G}$ and then converting it to the CDOS (see Eq. (S4)). In the case of a point-like scatterer and $\theta = \varepsilon_T$, the perturbation is $\Delta H = k^2 \Delta\varepsilon_T \delta(\mathbf{r} - \mathbf{r}_T)$, which results in

$$\mathcal{I}(\varepsilon_T, |u\rangle) = \frac{2\pi k^3}{\varepsilon_T} |\psi_u(\mathbf{r}_T)|^2 \rho(\mathbf{r}_T), \tag{S14}$$

for the Fisher information of an arbitrary incidence wavefront described by $|u\rangle$, with ψ_u being the resulting wave function. This shows that the scaling $\mathcal{I} \propto \rho^2$ comes from two contributions: The intensity at the target [5] and the unitarity of S. Both contribute a linear scaling of the QFI with the LDOS and together they result in $\mathcal{I} \propto \rho^2$. In the case of a non-unitary S matrix only a linear scaling of the QFI with the LDOS can therefore be observed [5].

The preceding result also readily solves another subtle point. The eigenvalues of F_θ fulfill the following identity in the unitary case , which follows from $F_\theta = Q_\theta^2$:

$$\Lambda = \langle\psi_u|\Delta H|\psi_u\rangle^2 / (4\Delta\theta^2), \tag{S15}$$

showing that eigenvalues scale quadratically with the intensity at the target while scaling linearly with the input intensity (which is $\propto \langle u|u\rangle$). Since the intensity at the target is proportional to the input intensity, this seems contradictory. Equation (S14) expresses the fact that different processes contribute to the intensity at the target position: the first contribution comes from the LDOS at the target position, while the second contribution is connected to the input intensity.

III. MAXIMUM QFI

Routine access to light's spatial degrees of freedom [6, 7] enables the generation of input fields that are spatially optimized to maximize the Fisher information [8]. This naturally leads to the question whether such a simple law as Eq. (4) also exists for such spatially-optimized input fields. In general, the QFI, first maximized over input fields and then averaged over the maxima of many disorder configurations, can be written as

$$\langle \mathcal{I}_\theta^{\max} \rangle = p_\theta N \langle \mathcal{I}_\theta^{\mathrm{avg}} \rangle, \tag{S16}$$

where $p_\theta = \langle\Lambda_1\rangle / \langle \mathrm{Tr}\, F_\theta \rangle$, with Λ_1 being the largest eigenvalue of F_θ. Note that Eq. (S16) is a simple reformulation of the identity $\langle \mathcal{I}_\theta^{\max} \rangle = 4\langle\Lambda_1\rangle$, which follows directly from $\mathcal{I}_\theta = 4\langle u|F_\theta|u\rangle$. In order to assess the benefits of maximizing the QFI over input fields, we need to determine the value of p_θ, which depends upon the parameter of interest.

On the one hand, for dielectric-constant estimations of a point-like target, we can write the following identity: $\mathrm{Tr}\, F_\varepsilon = \mathrm{Tr}\, Q_\varepsilon^2 = \mathrm{Tr}^2\, Q_\varepsilon$ (in line with what has been shown in Ref. [9]). This implies that the rank of F_ε is 1 regardless of the scattering environment, resulting in $p_\varepsilon = 1$. On the other hand, concerning estimations of the target's position, we can assess the value of p_x by studying the momentum delivered on the target by the probe field. Since, in the ballistic case, this momentum transfer can be applied both in the positive and negative x-direction, we can expect a value of 2 for the rank of F_x, resulting in $p_x = 0.5$. To confirm this reasoning, we use numerical simulations to calculate the ratios $\Lambda_1 / \mathrm{Tr}\, F_x$ and $\Lambda_2 / \mathrm{Tr}\, F_x$ (involving the largest and second largest eigenvalue $\Lambda_{1,2}$ of F_θ) for different disorder configurations and different scattering strength. In Fig. S1, we can see that these two quantities are, indeed, equal to 0.5 in the ballistic case, resulting in $p_x = 0.5$. However, adding a scattering environment around the particle breaks the directional symmetry, such that the normalized magnitudes of the two non-zero eigenvalues begin to bifurcate. An increase of the scattering strength leads to a stronger symmetry breaking; p_x thus increases with the scattering strength until it approaches its maximal value of $p_x = 1$ in the localized regime. The physical intuition emerging from these results is that the increase in QFI in the localized regime comes at the prize of reduced micro-manipulation capabilities (only one direction can be controlled).

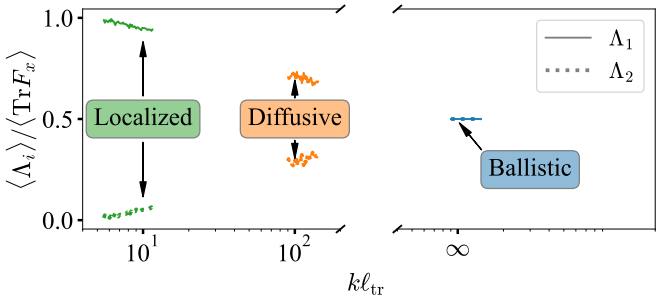

FIG. S1. Average normalized magnitude of the two largest eigenvalues, Λ_1, Λ_2, of F_x as a function of $k\ell_{\mathrm{tr}}$. In the ballistic regime, the rank of F_x is equal to 2, with equal contributions from the two non-zero eigenvalues ($\Lambda_1/\Lambda_2 \approx 1$). This symmetry breaks with increased scattering strength, resulting in an increased contribution from the largest eigenvalue in the diffusive and localized regimes. The numerical data used in this figure also underlies Figs. 2 and 3.

IV. SPECKLE CORRELATIONS

A central aspect of Eq. (4) in the main manuscript is that the average quantum Fisher information depends on the C_0–speckle correlation. We thus numerically studied the dependence of $C_0 = \mathrm{Var}[\rho(\mathbf{r}_T, k)] / \langle\rho(\mathbf{r}_T, k)\rangle^2$ upon the normalized transport mean free path $k\ell_{\mathrm{tr}}$. In the diffusive regime (for $k\ell_{\mathrm{tr}}$ of the order of 10^2), the C_0–speckle correlation is negligible ($C_0 \simeq 10^{-1}$), as shown in Fig. S2a. To check the influence of near-field effects around the target explicitly, we also performed nu-

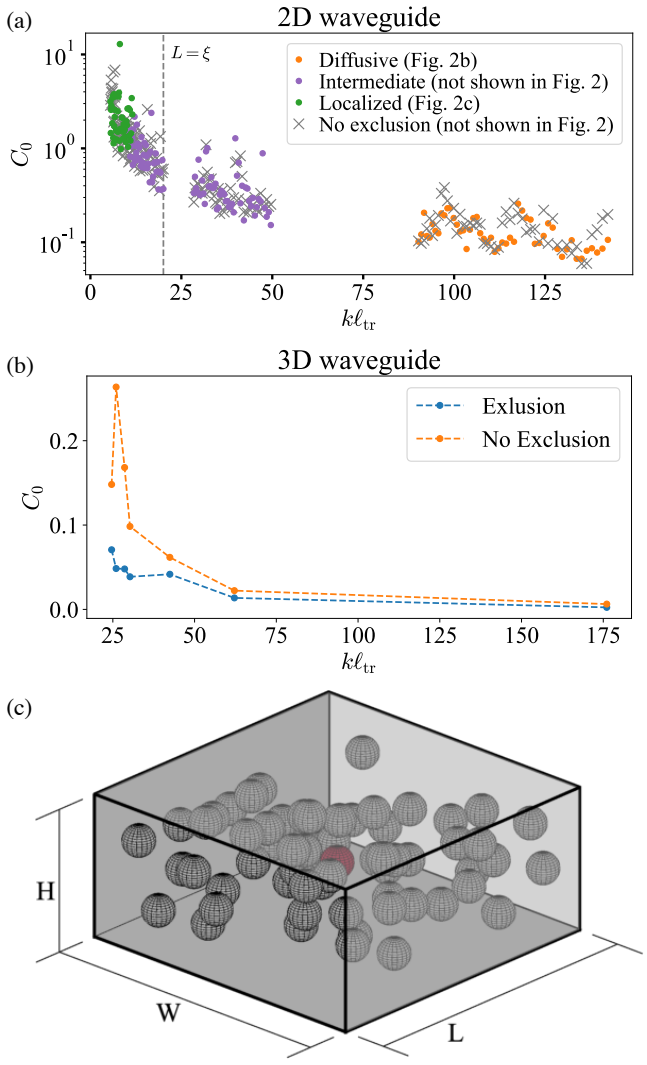

FIG. S2. (a) C_0–speckle correlation as a function of the normalised transport mean free path $k\ell_{\rm tr}$. Orange and green dots are obtained in the regimes considered in Fig. 2b and Fig. 2c of the manuscript, respectively. Purple dots are obtained from additional numerical simulations performed at the onset of the localized regime. Grey crosses are obtained in all regimes, but without an exclusion square around the target to capture near-field effects. The sharp increase of C_0 for small $k\ell_{\rm tr}$ explains the increase of the average quantum Fisher information observed in the localized regime (see Fig. 2c of the manuscript). Each dot is obtained after averaging over 100 random configurations. The vertical dashed grey line marks the onset of Anderson localization ($\xi = L$). (b) C_0–speckle correlation over $k\ell_{\rm tr}$ in 3D with an exclusion volume (blue) and without one (orange). We calculate each C_0-value from a sample with 50 randomly chosen configurations. The transport mean free path is estimated by using $\ell_{\rm tr} = L/(1 - \langle T\rangle)$, which is valid for $\langle T\rangle \gtrsim 0.5$. (c) Sketch of an example configuration in a waveguide of width W, length $L = W$ and height $H \approx 0.45W$. The scatterers (grey spheres) have hard walls, while the target (red sphere, not to scale) has refractive index $n = 1.44$. The frequency is set such that 8 transverse electric modes propagate inside the system.

merical calculations without the exclusion square around the target and find that there is only a $\simeq 15\%$ increase in C_0 in this diffusive regime. Both for the case with and without this exclusion region, we find that for decreasing $k\ell_{\rm tr}$, the value of C_0 increases significantly – there is, however, no discernible influence regarding the presence or absence of an exclusion region. When approaching the localized regime, the average quantum Fisher information increases with the scattering strength of the environment, as predicted from Eq. (4) and observed in Fig. 2c.

The effect of near-field interaction on the C_0 speckle correlations may be enhanced for 3D vector waves compared to 2D scalar waves. We thus numerically study the effect of the presence or absence of an exclusion volume on C_0 for vector waves in 3D (see Fig. S2b and c). Our model system is a multimode rectangular waveguide with hard walls in x and y-direction (the waves can enter and exit in z-direction). In this waveguide we place spheres with hard walls of radius $R = 0.05W$. We compute the LDOS at the center of a target scatterer with radius $R = 0.005W$, which is located at the waveguide's center position (in all three dimensions). The exclusion volume is a square of sidelength $0.4W$, which extends over the whole height of the waveguide. For systems with $k\ell_{\rm tr} \gtrsim 10^2$ (similar to the 2D diffusive case) we find that C_0 is still negligible both with and without an exclusion volume. More significant deviations are observed for $k\ell_{\rm tr} \ll 10^2$. This result can, however, be expected to depend on the choice of the scattering scenarios employed in the simulations: for point scatterers, or when resonances are excited, C_0 enhancements can be especially pronounced [10].

V. CONNECTION TO QCRB

The QCRB is log-normal distributed, $\Sigma_\theta \sim \text{Lognorm}(\mu, \sigma^2)$ [5]. This means that its inverse, which is the Fisher information, is also log-normal distributed with $\mu \to -\mu$, i.e., $\mathcal{I}_\theta \sim \text{Lognorm}(-\mu, \sigma^2)$. This implies that the average localization precision given by the QCRB is related to the Fisher information by

$$\langle \Sigma_\theta^{\rm avg}\rangle = e^{-2\mu}\langle \mathcal{I}_\theta^{\rm avg}\rangle, \tag{S17}$$

where $e^{-2\mu} = 2^4\langle \text{Tr}^2\, F_\theta\rangle / \langle \mathcal{I}_\theta^{\rm avg}\rangle^4 N^2$. In the case $\theta = x_T$ we get

$$e^{-2\mu} = \frac{2^6 N^2\left(\langle \rho_{11}^4\rangle - 2\langle \rho_{11}^2\rho_{12}^2\rangle + \langle \rho_{12}^4\rangle\right)}{k^{20}R^{16}(\varepsilon_T - 1)^4\pi^4(1 + C_0)^4\Delta x_T^4}, \tag{S18}$$

while for $\theta = \varepsilon_T$ we find

$$e^{-2\mu} = \frac{2^4 N^2\langle \rho(\mathbf{r}_T, k)^4\rangle}{k^{12}\varepsilon_T^4 R^{16}\pi^4(1 + C_0)^4}. \tag{S19}$$

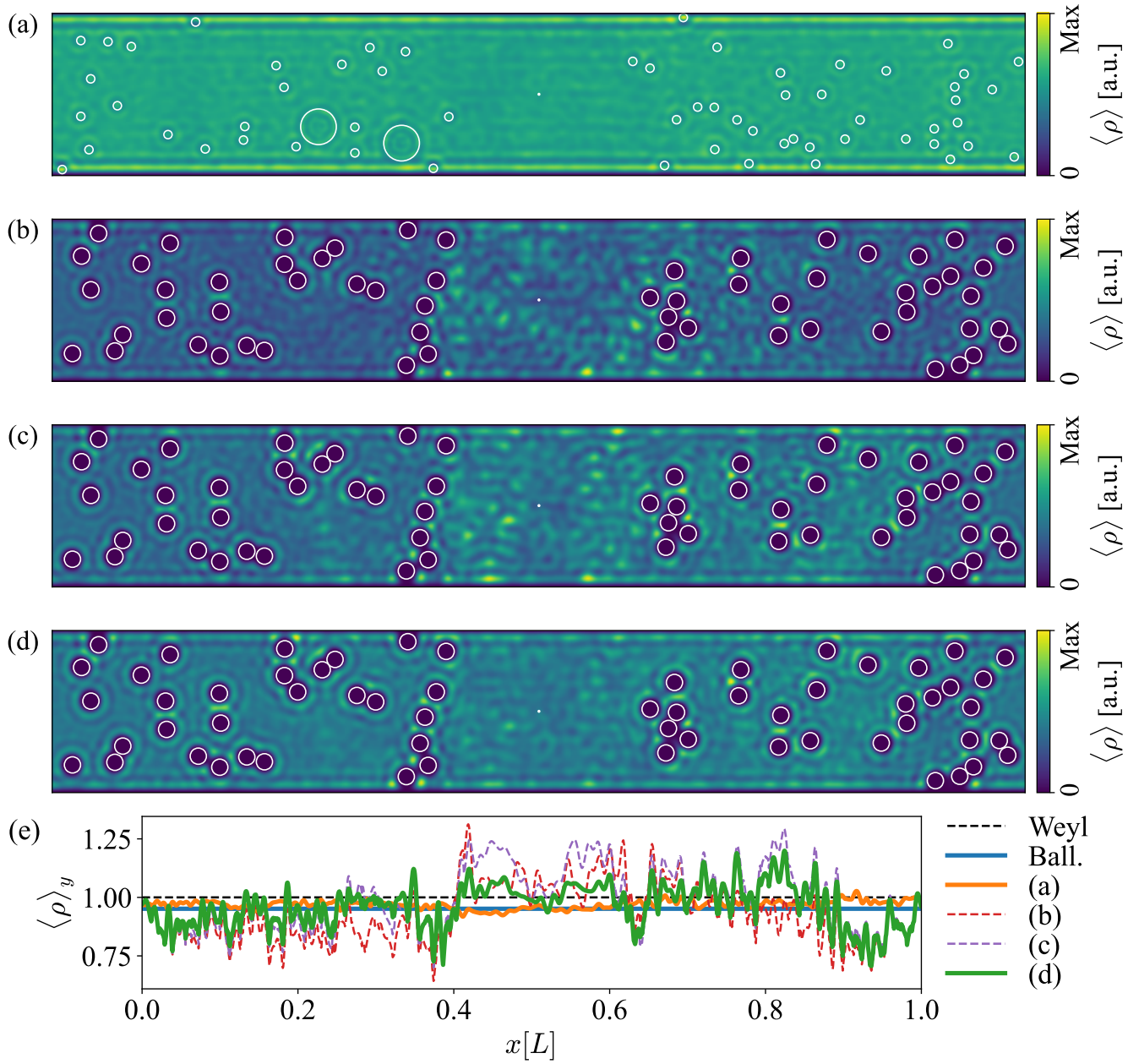

FIG. S3. Spatial distribution of the frequency-averaged LDOS $\langle\rho\rangle$ for the same geometry as depicted in (a) Fig. 2b (diffusive regime) or (b)-(d) Fig. 2c (localized regime) of the main text. (a) Frequency scan for $k \in [10.05, 14.95]\pi/W$ with a resolution of 50 points. (b)-(d) Progressively finer frequency scan for $k \in [10.025, 14.975]\pi/W$ with a resolution of (b) 50, (c) 95 and (d) 195 points (frequencies exactly at a transverse waveguide mode opening are discarded). (e) LDOS (normalized by the Weyl law) averaged over frequency and transversal direction $\langle\rho\rangle_y$ plotted over the longitudinal coordinate x. The Weyl law is the black dotted line. The blue line is the empty waveguide (the small decrease is due to boundary effects at the waveguide walls). Orange denotes the diffusive regime, while the red and violet dashed lines are the localized regime with 50 and 95 frequency points, respectively. The green line is the localized regime with 195 frequency points. Note that in the localized regime the impenetrable scatterers were removed from the averaging procedure for the LDOS at each value of x.

VI. UNIFORM DISTRIBUTION OF THE LDOS

An interesting result from the field of stochastic motion of classical particles is the insight that the average time that a particle undergoing a random walk inside a three-dimensional bounded system spends between entering and exiting this system is just determined by the ratio of the system's volume over its surface (or the area/circumference in 2D) [11]. This invariance of the average residence time or, equivalently "mean path length invariance" has meanwhile been generalized to wave scattering [12] and was observed in a corresponding experiment [13, 14].

Based on the work by Blanco and Fournier [11] it was later shown that the "mean path length" is not just an invariant for the system's entire scattering region, but, in fact, also for each of the system's sub-domains [15]. In other words, random walk trajectories entering a system from an external boundary feature an average length inside a chosen sub-domain of this system (like a region around a designated target) that is invariant with respect to the step size in the random walk process. For this average length it thus does not matter if the random walk trajectories are straight lines altogether or very convoluted paths. Apparently, when the step-size decreases the reduced likelihood for a part of the convoluted trajectories to even reach the target region is exactly compensated by the recurrent scattering of the remaining trajectories that increases their dwell time inside the target domain.

Similar to the translation of the global "mean path length invariance" to the domain of wave physics through the *global* DOS, we translate here the "mean path length invariance in every subdomain" to wave physics through the *local* DOS, which is the invariant quantity of interest here. Since the LDOS is derived from the full Green's function (see Eq. (S4)), it encompasses the full wave behavior including recurrent scattering. The invariance property of the LDOS manifests itself through the fact that it is spatially homogeneous upon frequency averaging. We confirm this with numerical simulations where we sum over the intensities for all input states at each point inside a single scattering geometry (see Fig. S3). In the diffusive regime the average intensities are equally distributed throughout the scattering region already for the 50 frequencies considered in Fig. 2 of the main text (apart from expected Friedel oscillations at the boundaries of the waveguide and the scattering centers). However, in the localized regime we need a finer resolution in the frequency domain to achieve spatial homogeneity for a single configuration (see the ever improving homogeneity in Fig. S3b-d). In the main text we compensate the coarser frequency scan with a larger number of scattering geometries.

VII. EFFECTS OF DISSIPATION

In order to analyze the effects of absorption we add a globally uniform imaginary part, n_I, to our system. This global and uniform absorption can also be modeled by shifting the frequency to $\omega + \mathrm{i}\alpha/2$, where $\alpha = 2kn_I$ is the absorption rate [16]. Under the assumption that $\alpha \ll \omega$ (corresponding to small dissipation) we can then expand the scattering matrix into

$$S_a(\omega + \mathrm{i}\alpha/2) \approx S(\omega)\left[\mathbb{1} - \frac{\alpha}{2}Q(\omega)\right], \tag{S20}$$

where Q is the Wigner-Smith time-delay operator and the subscript a denotes absorption (terms without it are evaluated at zero absorption). Plugging this into the Fisher information operator up to first order results in

$$F_{a,\theta} \approx F_\theta + \frac{\alpha}{2}\left(-\{Q, F_\theta\} + \mathrm{i}\left[Q_\theta, \frac{\mathrm{d}Q}{\mathrm{d}\theta}\right]\right), \tag{S21}$$

where $[\cdot,\cdot]$ ($\{\cdot,\cdot\}$) denotes the (anti-)commutator. Taking the trace results in the following simple expression since the trace over any commutator is zero:

$$\begin{aligned}\operatorname{Tr} F_{a,\theta} &\approx \operatorname{Tr} F_\theta - \alpha \operatorname{Tr}(QF_\theta), &\text{(S22)}\\ &= \operatorname{Tr} F_\theta - \alpha \sum_i \Lambda_i \langle f_i|Q|f_i\rangle, &\text{(S23)}\end{aligned}$$

where Λ_i and $|f_i\rangle$ denote the eigenvalues and eigenvectors of F_θ, respectively. This shows that the average QFI in the presence of small dissipation is the QFI without any absorption minus the weighted dwell-time of each FI-operator eigenstate. This confirms the intuitive picture that the average QFI is affected most if the dwell-time of states is large since those states are the ones that are most affected by absorption and hence also their interaction with the target. This analysis indirectly also confirms that the influence of absorption is particularly pronounced in the localized regime [17], since resonant localized states have particularly long dwell-times [12].

[1] M. Horodynski, M. Kühmayer, A. Brandstötter, K. Pichler, Y. V. Fyodorov, U. Kuhl, and S. Rotter, Nature Photonics **14**, 149 (2020).

[2] A. Cazé, R. Pierrat, and R. Carminati, Physical Review Letters **110**, 043823 (2013).

[3] A. Canaguier-Durand, R. Pierrat, and R. Carminati, Physical Review A **99**, 013835 (2019).

[4] P. de Vries, D. V. van Coevorden, and A. Lagendijk, Reviews of Modern Physics **70**, 447 (1998).

[5] D. Bouchet, R. Carminati, and A. P. Mosk, Physical Review Letters **124**, 133903 (2020).

[6] A. P. Mosk, A. Lagendijk, G. Lerosey, and M. Fink, Nat. Photonics **6**, 283 (2012).

[7] S. Rotter and S. Gigan, Reviews of Modern Physics **89**, 015005 (2017).

[8] D. Bouchet, S. Rotter, and A. P. Mosk, Nature Physics **17**, 564 (2021).
[9] P. del Hougne, K. B. Yeo, P. Besnier, and M. Davy, Physical Review Letters **126**, 193903 (2021).
[10] V. V. Marinyuk, Phys. Rev. A **104**, 023517 (2021).
[11] S. Blanco and R. Fournier, Europhysics Letters (EPL) **61**, 168 (2003).
[12] R. Pierrat, P. Ambichl, S. Gigan, A. Haber, R. Carminati, and S. Rotter, Proceedings of the National Academy of Sciences **111**, 17765 (2014).
[13] R. Savo, R. Pierrat, U. Najar, R. Carminati, S. Rotter, and S. Gigan, Science **358**, 765 (2017).
[14] M. Davy, M. Kühmayer, S. Gigan, and S. Rotter, Communications Physics **4**, 85 (2021).
[15] O. Bénichou, M. Coppey, M. Moreau, P. H. Suet, and R. Voituriez, Europhysics Letters (EPL) **70**, 42 (2005).
[16] C. Beenakker and P. Brouwer, Physica E: Low-dimensional Systems and Nanostructures **9**, 463 (2001).
[17] K. Y. Bliokh, Y. P. Bliokh, V. Freilikher, A. Z. Genack, B. Hu, and P. Sebbah, Physical Review Letters **97**, 243904 (2006).